Experimental Validation of a Kinetic Ballooning Mode in High-Performance High-Bootstrap Current Fraction Fusion Plasmas

X. Jian, J. Chen, S. Ding, A. Garofalo, X. Gong, C. Holland, J. Huang, V. S. Chan, X. Qin, G. Yu, R. R. Ma, X. Du, R. Hong, G. Staebler, H. Wang, Z. Yan, E. Bass, D. Brower, W. Ding, and D. Orlov

Phys. Rev. Lett. **131**, 145101 — Published 2 October 2023

DOI: 10.1103/PhysRevLett.131.145101

First Experimental Validation of a Kinetic Ballooning Mode in High Performance High Bootstrap Current Fraction Fusion Plasmas

X. Jian[1,2,3], J. Chen[4], S. Ding[1], A. Garofalo[1], X. Gong[2], C. Holland[3], J. Huang[2], V. S. Chan[1], X. Qin[5], G. Yu[6], R. Ma[7], X. Du[1], R. Hong[4], G. Staebler[1], H. Wang[1], Z. Yan[5], E. Bass[3], D. Brower[4], W. Ding[4], D. Orlov[3]

[1]General Atomics, P.O. Box 85608, San Diego, California 92186-5608, USA

[2]Institute of Plasma Physics, Chinese Academy of Sciences, Hefei, Anhui, China

[3]University of California, San Diego, La Jolla, California 92093-0417, USA

[4]University of California Los Angeles, Los Angeles, California 90095, USA

[5]University of Wisconsin-Madison, Madison, Wisconsin 53706, USA

[6]University of California at Davis, Davis, CA 95616, USA

[7]Southwestern Institute of Physics, P.O. Box 432 Chengdu 610041, China

Corresponding Email: juan.huang@ipp.ac.cn; xz_gong@ipp.ac.cn

Abstract: We report the observation of a set of coherent high frequency electromagnetic fluctuations that leads to a turbulence induced self-regulating phenomenon in the DIII-D high bootstrap current fraction plasma. The fluctuations have frequency of 130~220kHz, the poloidal wave length and phase velocity are 16~30 m^{-1} and ~30 km/s, respectively in the outboard midplane with the estimated toroidal mode number n~5-9. The fluctuations are located in the internal transport barrier (ITB) region at large radius and are experimentally validated to be kinetic ballooning modes (KBM). Quasi-linear estimation predicts the KBM to be able to drive experimental particle flux and non-negligible thermal flux, suggesting its significant role in regulating the ITB saturation.

1.Introduction

Fusion tokamak reactors are desired to operate in a fully non-inductive high-performance state[1]. Creation of an internal transport barrier[2-4] (ITB) can strongly elevate the plasma performance and facilitate steady-state operation by increasing the so-called 'bootstrap current' fraction f_{BS} ($= I_{BS}/I_P$, here I_{BS} and I_P are the bootstrap current and total plasma current, respectively)[5, 6]. The bootstrap current is spontaneously generated by the pressure gradient due to a toroidal geometry effect in tokamaks[7-9].

It is common wisdom that the high plasma pressure gradient in the ITB region can drive a broad range of micro-instabilities, like the ion temperature gradient mode (ITG)[10], trapped electron mode (TEM)[11, 12] and electron temperature gradient(ETG) mode[13] etc., which can efficiently drive thermal and/or particle transport and in turn limit the pressure gradient as a self-regulating process. Understanding the underlying mechanisms for the self-regulation of ITB is a strong leverage for optimization of fusion plasma performance and the verified dynamics could be generalized to other experimental conditions.

While ITG is amenable to strong electromagnetic stabilization and mean flow shearing, theory predicts electromagnetic turbulence, like micro-tearing modes (MTM)[14-16] and kinetic ballooning modes (KBM)[17, 18], can remain unstable and be particularly relevant for transport barriers in high performance plasmas. While the MTM is efficient in electron thermal transport, it has little effect on the other transport

channels (e.g., particle, ion thermal and momentum transport). KBM can drive transport in all channels in a highly stiff manner as predicted by theory and simulations, which argues for KBM being a strong candidate in setting a hard limit for the pressure gradient of transport barriers, even though an access to the 2nd stability region of KBM might be required as an intermediate process for the formation of transport barrier[19-21], like the H-mode pedestal[18]. By a phenomenological description, 'stiffness' means that the micro-instability can drive rapidly increasing transport flux once its threshold is reached[22, 23].

While KBM is frequently discussed and emphasized in the theory/simulation literature[24, 25], little experimental evidence is reported to support its role in the ITB saturation[26]. A convincing experimental validation effort requires the confluence of background profile information, as well as spatial and temporal fluctuation measurements throughout the evolution of the ITB, in addition to linear and nonlinear gyrokinetic simulations that quantitatively represent the experiment. Such confluence is rarely satisfied in a complex, large-scale experiment. The study reported herein is an exception. In this letter, 1) the first comprehensive experimental validation of the KBM in the core of DIII-D[27] high-performance high-f_{BS} plasmas is performed in the metric of mode eigenfunction, dispersion relation and toroidal mode number [26, 28]; 2) Quasi-linear estimation predicts the KBM can fully account for the experimental particle flux and contributes a non-negligible fraction of thermal flux, suggesting the importance of KBM in regulating the ITB saturation.

2.Experimental observations

The key fluctuations that are a signature of the KBM are observed in a DIII-D high f_{BS} discharge[5] (#185959, Fig. 1). Due to the enhanced confinement (Fig 1(b)), the line averaged density ($n_{e,line}$, Fig 1(c)) increases even though P_{NBI} drops a bit, suggesting the decrease of fast ion fraction. Specifically, n_f/n_e&P_f/P_{tot} drops from 0.038&0.19(t=2700ms) to 0.017&0.10(t=3350ms) at $\rho = 0.55$ (where the fluctuation peaks as will be discussed in section 3). n_f and P_f are estimated via NUBEAM code[29] with classical slowing down assumption of fast ions. Here ρ is a radial coordinate defined as the square root of the normalized toroidal magnetic flux, n_f and n_e is the fast ion density and electron density respectively while P_f is the fast ion pressure and P_{tot} the total pressure.

A new set of high frequency (130 kHz~220 kHz) coherent fluctuations (Fig 1(a)) appears in the top performance phase (TPP), t>2860ms marked by the red dashed line in Fig 1(b), which has lower P_f/P_{tot}, suggesting it is unlikely to be caused by fast ions. The plasma performance increment is mostly attributed to the enhancement of the ITB strength (P_{ITB}), rather than pedestal height (P_{ped}), as is evidenced by Fig 1(b) and 1(d), suggesting that the fluctuation excitation is likely related to core dynamics. Here $P_{ITB} = P_{\rho=0.3} - P_{\rho=0.7}, P_{ped} = P_{\rho=0.9}$ as defined in Fig 1(d), which shows both the pressure and q profiles of two representative time slices before(2700ms) and entry into(3350ms) the TPP. $P$is the total pressure of the thermal species. The enhancement of ITB is enabled by the buildup of a stronger density transport barrier (Fig 1(e)). The temperature profiles are roughly unchanged, with on-axis value of 2.7 and 3.5keV for

electron (Fig 1(f)) and ion channels (Fig 1(g)), respectively.

Both theoretical and experimental analysis indicate that the ITB attainment mostly relies on the α(~dP/dr) stabilization of drift-wave instabilities[30-34], which is a spontaneous turbulence stabilization effect coming from modification of the magnetic drift frequency, rather than the toroidal rotation shear, which is expected to be small in future machines[35]. With a strong ITB, the plasma performance reaches a very high level with relevant global parameters in the TPP (t=3350 ms, Fig 1(b)) shown in Table I. Here, B_T is the external imposed toroidal magnetic field at the tokamak geometry center, q_{95} is the safety factor at 95% of the normalized poloidal flux, $H_{98(y,2)} = \tau_E/\tau_{E,th}^{IPB98(y,2)}$, with τ_E being the energy confinement time and $\tau_{E,th}^{IPB98(y,2)}$ a parametric scaling of energy confinement time based on a multi-machine database[36]. $\beta_N = \beta_t/(I_p/aB_T)$ with $\beta_t = \frac{2\mu_0 p}{B_T^2}$, $\beta_p = \frac{2\mu_0 p}{B_p^2}$, μ_0 is the vacuum magnetic permeability, p, a and B_p is the total plasma pressure, plasma minor radius and the poloidal magnetic field, respectively. The quantity f_{NI} is the non-inductive current fraction (sum over both the bootstrap current and external driven current), and $f_{GW} = n_{e,line}/n_{e,GW}$ with $n_{e,GW}$ the Greenwald density limit. The compatibility of good confinement ($H_{98(y,2)}$=1.7), good MHD stability (β_N=4.2), high f_{BS}(=80%, calculated by Sauter model[7]), high f_{GW} and compatibility with an edge exhaust solution[21] makes such a scenario highly attractive for the steady state operation of future fusion reactors. In addition, several global parameters (e.g., $H_{98(y,2)}$, β_N, β_p, f_{BS}) have reached or exceeded the desired range for some attractive fusion power plant(FPP) designs[37-41]. Although the equivalent fusion gain $Q_{DT,equivlent}$ is only ~0.01 for this DIII-D discharge since the T_i value is low, extrapolating such a discharge with reasonable additional assumptions to the proposed fusion test reactor CFETR[42] suggests that a fusion gain of 15.0 can be achieved according to systems code(GASC[43]) estimation, highlighting the relevance of transport physics in this discharge to the FPP.

Table I. Global plasma parameters at t=3350ms

I_p(MA)/B_T(T)	$q_{95}/H_{98(y,2)}$	β_N/β_p	f_{BS}/f_{NI}	f_{GW}
0.78/1.7	7.7/1.7	4.2/3.0	80%/95%	1.01

The fluctuation signal comes from the crosspower between the line integral measurement of density and magnetic fluctuations of the Radial Interferometer Polarimeter (RIP)[44, 45], more elaborate calculations suggest the mode has $(\delta B_r/B_T)/(\delta n_e/n_e)$~0.1, which is comparable to the value of pedestal micro-tearing modes[44-48], suggesting the magnetic nature of such a mode. Here δB_r is defined as the root mean square line-averaged magnetic fluctuation amplitude[45] with $\delta B_r/B_T$~10^{-4}, $\delta n_e/n_e$(~10^{-3}) is the normalized density fluctuation coming from local beam emission spectroscopy (BES)[49] measurement with more details shown in the next section.

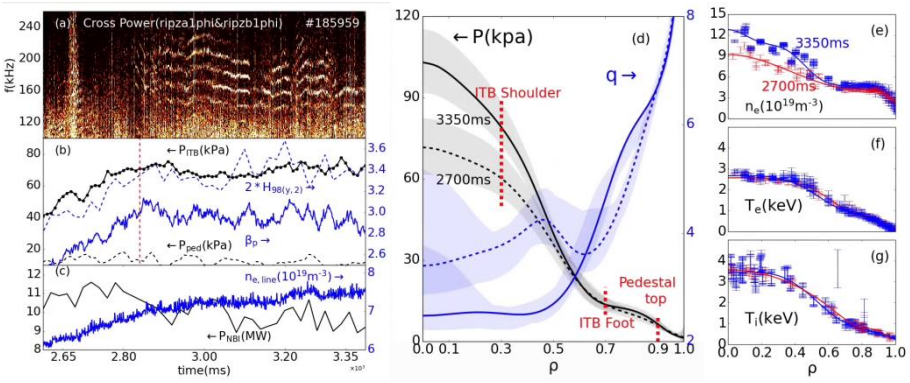

Figure 1(a), The correlation frequency spectrum between the RIP density and magnetic measurement, (b) temporal evolution of the ITB strength (black dotted), pedestal height (black dashed line), $H_{98(y,2)}$(blue dashed) and β_p(blue solid), (c) temporal evolution of NBI power(P_{NBI}) and line averaged density($n_{e,line}$) (d) profiles of thermal pressure(black) and safety factor q(blue) before (t=2700ms, dashed) and after (t=3350ms, solid) the fluctuation onset with uncertainties marked with shadows. Kinetic profiles of (e) electron density n_e, (f) electron temperature T_e and (g) ion temperature T_i of t=2700ms(red) and t=3350ms(blue)

3.Fluctuation Characteristics and Comparison with Theory & Simulation

In this section, it will be demonstrated that the experimental features of the fluctuations are consistent with the theoretical expectations of KBM[50] in the following metrics: mode location, dispersion relation and toroidal mode number.

Mode location. The eigenfunction of the radial perturbation displacement ξ_r of the fluctuations (Fig 1(a)) is inferred based on the following expression[51, 52]

$$\frac{\delta n_e}{n_e} = -\nabla \cdot \vec{\xi} - \vec{\xi} \cdot \frac{\nabla n_e}{n_e} \tag{1}$$

Here, we ignore the compression term $(\nabla \cdot \xi)$ and then have

$$|\xi_r| = |\frac{\delta n_e}{n_e}| \ \frac{n_e}{-\nabla n_e} \tag{2}$$

The use of Eq. (2) should suffice for our goals since we are mostly interested in the rough position of the mode location rather than the accurate amplitude of ξ_r. Here, $\frac{\delta n_e}{n_e}$ is measured by the BES system on DIII-D, which spans over $\rho = [0.5,0.7]$ for this discharge. Specifically, it can be calculated by integrating the fluctuating density cross power between poloidally displaced channels pairs ($\Delta Z \sim 1.5$ cm in the same magnetic surface) over the frequency range of 130 to 220 kHz, which is the relevant frequency range of such a mode and averaging from 3000 to 3400 ms. By repeating the calculation for each poloidally displaced BES channel pair along the radial direction, the $|\frac{\delta n_e}{n_e}|$ profile can be obtained. The equilibrium density profile n_e is measured via Thomson scattering[53] and its gradient ∇n_e is estimated from a dedicated profile fitting tool OMFITProfiles[54] in the OMFIT framework[55]. With $|\frac{\delta n_e}{n_e}|$ and $\frac{n_e}{-\nabla n_e}$ information

obtained, based on Eq. (2), the $|\delta\xi_r|$ is estimated to locate in the ITB region and peaks at ρ = 0.55(Fig 2(a)), consistent with the inference in section 2 that the mode is correlated with core dynamics rather than edge.

For quantitative validation, our approach here is to perform multiple linear ion-scale ($k_y\rho_s$<1, here $k_y = nq/r$ is the poloidal wave number with n, q and r the toroidal mode number, safety factor and the minor radius, respectively[56], ρ_s is the gyroradius of ion sound velocity c_s) flux-tube gyrokinetic simulations (with measured profiles at t=3350 ms) across the desire radial range using the high-fidelity gyrokinetic code CGYRO[57]. It predicts the KBM to be robustly unstable within the ITB region and has the largest growth rate at ρ = 0.55 (Fig. 2(b), consistent with the measured eigenfunction shown in Fig 2(a). These calculations have been verified against independent calculations made with GYRO[58], which uses different coordinate grids and numerical algorithms than CGYRO. Comparison with global models for further validation is left for future study.

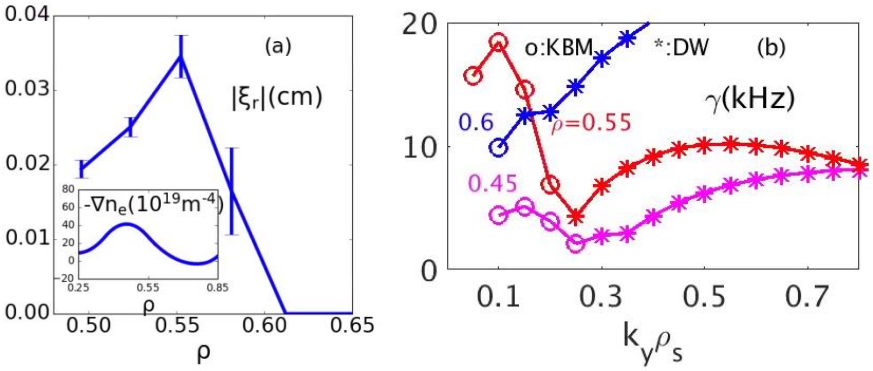

Figure 2 (a) the amplitude of eigenfunction $\delta\xi_r$, with density gradient plotted alongside, (b) the linear growth rate spectrum at different radii. The KBM is denoted with circles(o) while the asterisk (*) represents the drift wave instabilities

Mode dispersion relation. The coherence (Fig 3(a)) and the cross phase (Fig 3 (b)) of two poloidally displaced BES channels located at $\rho = 0.55$ are presented, from which the phase velocity of fluctuations is estimated to be ~30 km/s at the outboard midplane. Poloidal channels which have the largest poloidal separation (ΔZ~0.1 m) are chosen to reduce the uncertainties in the cross-phase, and hence the phase velocity calculation.

The estimated phase velocity(V_{BES}) matches the sum (V_{tot}) of ion diamagnetic velocity (V_{*pi}) and $E_r \times B$ velocity (V_{Er}) within the BES error bar (~12%, denoted by the purple shadow) at ρ = 0.55 (Fig 3(c)), consistent with theoretical expectation of the KBM dispersion (which has phase velocity of order the ion diamagnetic velocity and propagating in the ion diamagnetic direction)[50] and the mode location inferred in Fig 2(a).

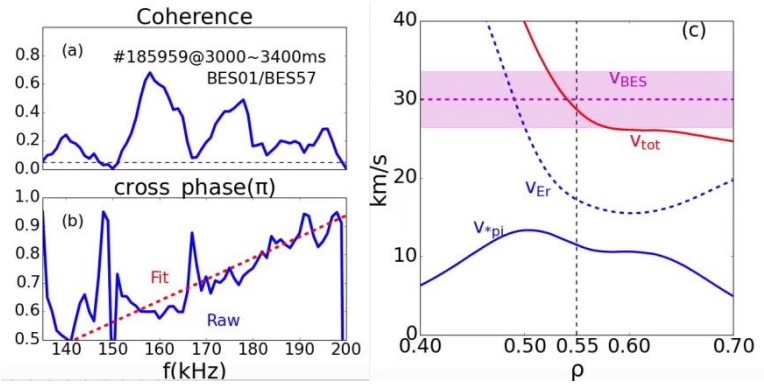

Figure 3. (a) coherence and (b) cross phase between two BES channels at $\rho = 0.55$; (c) the background $E_r \times B$ velocity (V_{Er}, blue dashed), diamagnetic velocity (V_{*pi}, blue solid) and the sum of them (V_{tot}, red). The mode phase velocity inferred from BES (V_{BES}) is represented with purple dashed line with the uncertainties denoted with purple shadows

Toroidal Mode number. Theories predict that the beam-like KBM with $k_y \rho_s$ satisfying $\omega_{*pi} \sim \omega_{GAM}$ will strongly react with geodesic acoustic mode(GAM[59, 60]), gaining energy and become most unstable (least stable) [50], here ω_{*pi} and ω_{GAM} are the ion diamagnetic frequency and GAM frequency, respectively. With this, the most unstable mode is predicted to have $k_y \rho_s \sim 0.1$ (consistent with CGYRO linear spectrum shown in Fig. 2(b)) and n~6 across the peak gradient region (ρ= [0.4,0.6]) as plotted in Fig 4. BES analysis of the mode with the strongest coherence (frequency~158 kHz, also has the highest amplitude) in Fig 3(a) shows it has wave number $k_{y,loc} \sim 20$ m^{-1} at the outboard midplane, which corresponds to n~6 and agrees well with the theoretical prediction[50] very well. Here n is estimated via

$$n = r k_{y,loc}/q_{loc} \quad (3).$$

Here $q_{loc}(=\frac{dv}{d\theta}$, where v is the eikonal phase function as defined in Ref[40], while θ is the generalized poloidal angle) is the local q value (of $\rho = 0.55$), which is poloidal-angle dependent, at the outboard midplane where the BES locates. With Eq. (3), the n of the other harmonics shown in Fig 3(a) can be similarly estimated and it shows that n=5~9 is excited (represented by the blue shadow in Fig 4), consistent with theoretical predictions.

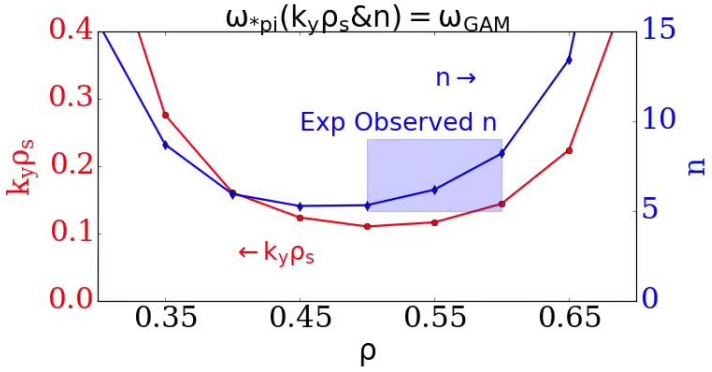

Figure 4. The $k_y\rho_s$ (red) and n (blue) that enables $\omega_{*pi} = \omega_{GAM}$. Experimentally observed toroidal mode number in the BES detected radial range is represented with blue shadow

4. Transport capability

The transport capability of the mode is quantified to address the role of KBM in the ITB saturation. Here we employed a quasi-linear approach[61], with the fluctuation intensity coming from the BES measurements (Fig 5(a)) and the quasi-linear weight from the linear CGYRO calculation of $\rho = 0.55$ (Fig 5(b), which has gyroradius ρ_s= 2.2mm (corresponding to the normalized gyroradius $\frac{\rho_s}{a}$ = 3.8e-3). The validity of the quasi-linear approach is justified based on the fact that the density fluctuation intensity is comparable to $\frac{\rho_s}{a}$, with both quantities in the order of 10^{-3}. By assuming $\frac{e\delta\phi}{T_e} = \frac{\delta n_e}{n_e}$ (here $\delta\phi$ is the fluctuating electrostatic potential), the flux spectrum can then be obtained (Fig 5(c)). Sum of the flux contributed by each toroidal mode gives the total flux for each transport channel (Fig 5(d)). KBMs are shown to be able to account for almost all the particle flux and non-negligible fractions of thermal fluxes. Initial encounter of KBM is enabled by the combination of bootstrap and inductive current evolution resulting in magnetic shear changes from negative to positive at ρ=0.55 (Fig1 (d)) and the density increase, as evidence by the CGYRO calculation, which predicts both the growth rate and quasi-linear weight of particle flux to increase with enhancement of $a/L_{ne}(= -\frac{a}{n_e}\frac{dn_e}{dr}$, calculation is based on n=6, Fig 5(e).), indicating the strong capability of KBM for regulating the density profile in the temporal dynamic of the TPP(Fig 1 (c)), which is also consistent with the saturation of density profile after the KBM onset. Note Fig 5(e) is calculated with self-consistent α and Shafranov shift values. It would be worthwhile to mention that while α(~dP/dr) is stabilizing, Grad-Shafranov shift, which is proportional to the β_p value in a given enclosed magnetic surface and generally increase with local α in real experiments, is destabilizing due to the widening of the bad curvature. More details will be discussed elsewhere. Since ~50% of the pressure gradient is contributed by the density gradient for this discharge

($F_n = \frac{T\nabla n}{\nabla p} = \frac{T\nabla n}{T\nabla n + n\nabla T}$~50%), it is therefore justifiable to conclude that the KBM plays a significant role in regulating the ITB strength.

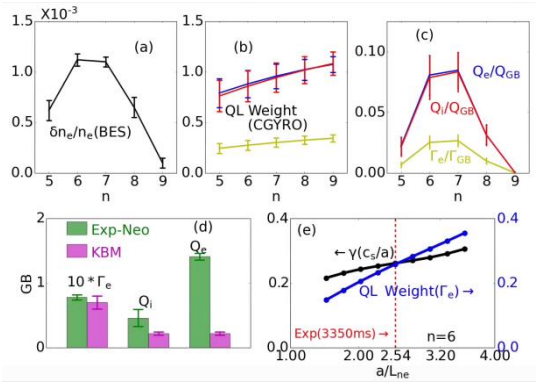

Figure 5. (a) density fluctuation amplitude measured by BES at $\rho = 0.55$ for each toroidal mode; (b) the quasi-linear weight of different transport channels from linear CGYRO simulation, error bar comes from the consideration of uncertainties in magnetic shear; (c) estimated quasi-linear flux spectrum; (d) comparison between the gyrobohm normalized quasi-linear flux and the power balance value. The green bars denotes the flux obtained via subtracting the neoclassical transport contribution (calculated by the NEO[62, 63] code) from the power balance value (estimated via the TRANSP code[64, 65]) while the KBM induced transport is represented by the purple bars. (e) The dependence of quasi-linear weight of electron particle flux (blue) and growth rate (black) on a/L_{ne}, calculation is based background parameters of t=3350ms

5. Conclusion & Discussion

A self-regulating phenomenon induced by high frequency core coherent magnetic and density fluctuations is identified for the first time, in the ITB region of a DIII-D high-performance high bootstrap current fraction plasma. The experimental features of the fluctuation are in quantitative agreement with gyrokinetic theory and two state-of-the-art gyrokinetic models for KBMs. Quasi-linear estimation of the fluctuation induced flux is comparable to the experimental power balance value (especially for the particle channel), suggesting its important role in the ITB self-regulation process，in which the experimental appearance of the KBM fluctuations can be correlated with the saturation of plasma performance. Our work provides a blueprint for future experiments to confirm the robust role of KBM in ITB saturation of high confinement plasmas, and to explore self-regulating phenomena in other transport channels.

Acknowledgement

Discussions with Y. Zou in SWIP, T. Rhodes in UCLA, G. McKee in UW Madison, P. J. Sun in ASIPP, Z. Li and J. Candy in General Atomics are appreciated. We also appreciate the anonymous referees for many helpful suggestions. This work was supported by the U.S. Department of Energy under Award Nos. DE-SC0018287, DE-SC0017992, DE-FG02-95ER54309, DE-SC0019004, DE-FG02-08ER54999, DE-FG02-99ER54531, DE-SC0019352 and DE-FC02-04ER54698. This research

used resources of the National Energy Research Scientific Computing Center (NERSC); a U.S. Department of Energy Office of Science User Facility operated under Contract No. DEAC02-05CH11231 using NERSC award ERCAP0020598.

References

1. C. Gormezano, A. C. C. Sips, T. C. Luce, S. Ide, A. Becoulet, X. Litaudon, A. Isayama, J. Hobirk, M. R. Wade and T. Oikawa, Nuclear Fusion **47** (6), S285 (2007).
2. J. W. Connor, T. Fukuda, X. Garbet, C. Gormezano, V. Mukhovatov and M. Wakatani, Nuclear Fusion **44** (4), R1 (2004).
3. K. Ida and T. Fujita, Plasma Physics and Controlled Fusion **60** (3), 033001 (2018).
4. O. Gruber, R. C. Wolf, R. Dux, C. Fuchs, S. Günter, A. Kallenbach, K. Lackner, M. Maraschek, P. J. McCarthy and H. Meister, Physical review letters **83** (9), 1787 (1999).
5. A. M. Garofalo, X. Gong, B. A. Grierson, Q. Ren, W. M. Solomon, E. J. Strait, M. A. Van Zeeland, C. T. Holcomb, O. Meneghini and S. P. Smith, Nuclear Fusion **55** (12), 123025 (2015).
6. T. Fujita, S. Ide, Y. Kamada, T. Suzuki, T. Oikawa, S. Takeji, Y. Sakamoto, Y. Koide, A. Isayama and T. Hatae, Physical review letters **87** (8), 085001 (2001).
7. O. Sauter, C. Angioni and Y. R. Lin-Liu, Physics of Plasmas **6** (7), 2834-2839 (1999).
8. A. G. Peeters, Plasma Physics and Controlled Fusion **42** (12B), B231 (2000).
9. W. A. Houlberg, K.-C. Shaing, S. P. Hirshman and M. C. Zarnstorff, Physics of Plasmas **4** (9), 3230-3242 (1997).
10. F. Romanelli, Physics of Fluids B: Plasma Physics **1** (5), 1018-1025 (1989).
11. T. Dannert and F. Jenko, Physics of Plasmas **12** (7), 072309 (2005).
12. S. Ding, X. Jian, A. M. Garofalo, Z. Yan, J. McClenaghan, W. Guo and B. A. Grierson, Nuclear Fusion **60** (1), 016023 (2019).
13. F. Jenko, W. Dorland and G. W. Hammett, Physics of Plasmas **8** (9), 4096-4104 (2001).
14. J. F. Drake and Y. C. Lee, The Physics of Fluids **20** (8), 1341-1353 (1977).
15. W. Guttenfelder, J. Candy, S. M. Kaye, W. M. Nevins, E. Wang, R. E. Bell, G. W. Hammett, B. P. LeBlanc, D. R. Mikkelsen and H. Yuh, Physical review letters **106** (15), 155004 (2011).
16. X. Jian, C. Holland, J. Candy, E. Belli, V. Chan, A. M. Garofalo and S. Ding, Physical Review Letters **123** (22), 225002 (2019).
17. M. J. Pueschel and F. Jenko, Physics of Plasmas **17** (6), 062307 (2010).
18. P. B. Snyder, R. J. Groebner, J. W. Hughes, T. H. Osborne, M. Beurskens, A. W. Leonard, H. R. Wilson and X. Q. Xu, Nuclear Fusion **51** (10), 103016 (2011).

19. S. Saarelma, M. E. Austin, M. Knolker, A. Marinoni, C. Paz-Soldan, L. Schmitz and P. B. Snyder, Plasma Physics and Controlled Fusion **63** (10), 105006 (2021).
20. G. M. Staebler, A. M. Garofalo, C. Pan, J. McClenaghan, M. A. Van Zeeland and L. L. Lao, Physics of Plasmas **25** (5), 056113 (2018).
21. L. Wang, H. Q. Wang, S. Ding, A. M. Garofalo, X. Z. Gong, D. Eldon, H. Y. Guo, A. W. Leonard, A. W. Hyatt and J. P. Qian, Nature communications **12** (1), 1-9 (2021).
22. C. Holland, T. C. Luce, B. A. Grierson, S. P. Smith, A. Marinoni, K. H. Burrell, C. C. Petty and E. M. Bass, Nuclear Fusion **61** (6), 066033 (2021).
23. T. C. Luce, K. H. Burrell, C. Holland, A. Marinoni, C. C. Petty, S. P. Smith, M. E. Austin, B. A. Grierson and L. Zeng, Nuclear Fusion **58** (2), 026023 (2018).
24. P. B. Snyder and G. W. Hammett, Physics of Plasmas **8** (3), 744-749 (2001).
25. N. Kumar, Y. Camenen, S. Benkadda, C. Bourdelle, A. Loarte, A. R. Polevoi and F. Widmer, Nuclear Fusion **61** (3), 036005 (2021).
26. Z. Yan, G. R. McKee, R. J. Groebner, P. B. Snyder, T. H. Osborne and K. H. Burrell, Physical review letters **107** (5), 055004 (2011).
27. J. L. Luxon, Nuclear Fusion **42** (5), 614 (2002).
28. X. D. Du, R. J. Hong, W. W. Heidbrink, X. Jian, H. Wang, N. W. Eidietis, M. A. Van Zeeland, M. E. Austin, Y. Liu and N. A. Crocker, Physical Review Letters **127** (2), 025001 (2021).
29. A. Pankin, D. McCune, R. Andre, G. Bateman and A. Kritz, Computer Physics Communications **159** (3), 157-184 (2004).
30. C. Bourdelle, G. T. Hoang, X. Litaudon, C. M. Roach and T. Tala, Nuclear fusion **45** (2), 110 (2005).
31. S. Ding, A. M. Garofalo, J. Qian, L. Cui, J. T. McClenaghan, C. Pan, J. Chen, X. Zhai, G. McKee and Q. Ren, Physics of Plasmas **24** (5), 056114 (2017).
32. K. Itoh, S. I. Itoh, A. Fukuyama, M. Yagi and M. Azumi, Plasma physics and controlled fusion **36** (2), 279 (1994).
33. S.-I. Itoh, K. Itoh, M. Yagi and A. Fukuyama, Plasma physics and controlled fusion **38** (10), 1743 (1996).
34. M. A. Beer, G. W. Hammett, G. Rewoldt, E. J. Synakowski, M. C. Zarnstorff and W. Dorland, Physics of Plasmas **4** (5), 1792-1799 (1997).
35. C. Chrystal, B. A. Grierson, S. R. Haskey, A. C. Sontag, F. M. Poli, M. W. Shafer and J. S. Degrassie, Nuclear Fusion **60** (3), 036003 (2020).
36. M. Shimada, D. J. Campbell, V. Mukhovatov, M. Fujiwara, N. Kirneva, K. Lackner, M. Nagami, V. D. Pustovitov, N. Uckan, J. Wesley, N. Asakura, A. E. Costley, A. J. H. Donné, E. J. Doyle, A. Fasoli, C. Gormezano, Y. Gribov, O. Gruber, T. C. Hender, W. Houlberg, S. Ide, Y. Kamada, A. Leonard, B. Lipschultz, A. Loarte, K. Miyamoto, V. Mukhovatov, T. H. Osborne, A. Polevoi and A. C. C. Sips, Nuclear Fusion **47** (6), S1-S17 (2007).
37. M. Kikuchi, Y. Seki and K. Nakagawa, Fusion engineering and design **48** (3-4), 265-270 (2000).
38. K. Tobita, S. Nishio, M. Enoeda, M. Sato, T. Isono, S. Sakurai, H. Nakamura, S. Sato, S. Suzuki and M. Ando, Fusion Engineering and Design **81** (8-14), 1151-1158 (2006).
39. C. E. Kessel, F. M. Poli, K. Ghantous, N. N. Gorelenkov, M. E. Rensink, T. D. Rognlien, P. B. Snyder, H. S. John and A. D. Turnbull, Fusion Science and Technology **67** (1), 75-106 (2015).
40. M. Kikuchi, Nuclear fusion **30** (2), 265 (1990).
41. A. M. Garofalo, M. A. Abdou, J. M. Canik, V. S. Chan, A. W. Hyatt, D. N. Hill, N. B. Morley, G. A. Navratil, M. E. Sawan and T. S. Taylor, Fusion Engineering and Design **89** (7-8), 876-881 (2014).

42. J. Chen, V. S. Chan, X. Jian, X. Zhang, Q. Ren, G. Li and C. Zhou, Nuclear Fusion **61** (4), 046002 (2021).
43. V. S. Chan, R. D. Stambaugh, A. M. Garofalo, M. S. Chu, R. K. Fisher, C. M. Greenfield, D. A. Humphreys, L. L. Lao, J. A. Leuer and T. W. Petrie, Fusion Science and Technology **57** (1), 66-93 (2010).
44. J. Chen, D. L. Brower, W. X. Ding, Z. Yan, T. Osborne, E. Strait, M. Curie, D. R. Hatch, M. Kotschenreuther and X. Jian, Physics of Plasmas **27** (12), 120701 (2020).
45. J. Chen, D. L. Brower, W. X. Ding, Z. Yan, M. Curie, M. Kotschenreuther, T. Osborne, E. Strait, D. R. Hatch and M. R. Halfmoon, Physics of Plasmas **28** (2), 022506 (2021).
46. D. R. Hatch, M. Kotschenreuther, S. Mahajan, P. Valanju and X. Liu, Nuclear Fusion **57** (3), 036020 (2017).
47. D. R. Hatch, M. Kotschenreuther, S. Mahajan, P. Valanju, F. Jenko, D. Told, T. Görler and S. Saarelma, Nuclear Fusion **56** (10), 104003 (2016).
48. M. Kotschenreuther, X. Liu, D. R. Hatch, S. Mahajan, L. Zheng, A. Diallo, R. Groebner, J. C. Hillesheim, C. F. Maggi and C. Giroud, Nuclear Fusion **59** (9), 096001 (2019).
49. G. R. McKee, R. J. Fonck, D. K. Gupta, D. J. Schlossberg, M. W. Shafer, R. L. Boivin and W. Solomon, Plasma and Fusion Research **2**, S1025-S1025 (2007).
50. F. Zonca, L. Chen and R. A. Santoro, Plasma physics and controlled fusion **38** (11), 2011 (1996).
51. M. A. Van Zeeland, G. J. Kramer, M. E. Austin, R. L. Boivin, W. W. Heidbrink, M. A. Makowski, G. R. McKee, R. Nazikian, W. M. Solomon and G. Wang, Physical review letters **97** (13), 135001 (2006).
52. R. Nazikian, G. J. Kramer, C. Z. Cheng, N. N. Gorelenkov, H. L. Berk and S. E. Sharapov, Physical review letters **91** (12), 125003 (2003).
53. D. M. Ponce-Marquez, B. D. Bray, T. M. Deterly, C. Liu and D. Eldon, Review of Scientific Instruments **81** (10), 10D525 (2010).
54. N. C. Logan, B. A. Grierson, S. R. Haskey, S. P. Smith, O. Meneghini and D. Eldon, Fusion Science and Technology **74** (1-2), 125-134 (2018).
55. O. Meneghini, S. P. Smith, L. L. Lao, O. Izacard, Q. Ren, J. M. Park, J. Candy, Z. Wang, C. J. Luna and V. A. Izzo, Nuclear Fusion **55** (8), 083008 (2015).
56. J. Candy, Plasma Physics and Controlled Fusion **51** (10), 105009 (2009).
57. J. Candy, E. A. Belli and R. V. Bravenec, Journal of Computational Physics **324**, 73-93 (2016).
58. J. Candy and R. E. Waltz, Journal of Computational Physics **186** (2), 545-581 (2003).
59. N. Winsor, J. L. Johnson and J. M. Dawson, The Physics of Fluids **11** (11), 2448-2450 (1968).
60. G. D. Conway, A. I. Smolyakov and T. Ido, Nuclear Fusion (2021).
61. J. E. Kinsey, G. M. Staebler and R. E. Waltz, Physics of Plasmas **15** (5), 055908 (2008).
62. E. A. Belli and J. Candy, Plasma Physics and Controlled Fusion **50** (9), 095010 (2008).
63. E. A. Belli and J. Candy, Plasma Physics and Controlled Fusion **51** (7), 075018 (2009).
64. R. J. Hawryluk, in *Physics of plasmas close to thermonuclear conditions* (Elsevier, 1981), pp. 19-46.
65. B. A. Grierson, X. Yuan, M. Gorelenkova, S. Kaye, N. C. Logan, O. Meneghini, S. R. Haskey, J. Buchanan, M. Fitzgerald and S. P. Smith, Fusion Science and Technology **74** (1-2), 101-115 (2018).